

Ultra-thin alumina and silicon nitride MEMS fabricated membranes for the electron multiplication

Prodanović, V.; Chan, H.W.; van der Graaf, H.; Sarro, P.M.

DOI

[10.1088/1361-6528/aaac66](https://doi.org/10.1088/1361-6528/aaac66)

Publication date

2018

Document Version

Final published version

Published in

Nanotechnology

Citation (APA)

Prodanović, V., Chan, H. W., van der Graaf, H., & Sarro, P. M. (2018). Ultra-thin alumina and silicon nitride MEMS fabricated membranes for the electron multiplication. *Nanotechnology*, 29(15), 1-11. Article 155703. <https://doi.org/10.1088/1361-6528/aaac66>

Important note

To cite this publication, please use the final published version (if applicable). Please check the document version above.

Copyright

Other than for strictly personal use, it is not permitted to download, forward or distribute the text or part of it, without the consent of the author(s) and/or copyright holder(s), unless the work is under an open content license such as Creative Commons.

Takedown policy

Please contact us and provide details if you believe this document breaches copyrights. We will remove access to the work immediately and investigate your claim.

Green Open Access added to TU Delft Institutional Repository

'You share, we take care!' - Taverne project

<https://www.openaccess.nl/en/you-share-we-take-care>

Otherwise as indicated in the copyright section: the publisher is the copyright holder of this work and the author uses the Dutch legislation to make this work public.

PAPER

Ultra-thin alumina and silicon nitride MEMS fabricated membranes for the electron multiplication

To cite this article: V Prodanovi *et al* 2018 *Nanotechnology* **29** 155703

View the [article online](#) for updates and enhancements.

Related content

- [Suspended nanostructured alumina membranes](#)
Lauri Sainiemi, Kostas Grigoras and Sami Franssila
- [In situ spectroscopic ellipsometry as a versatile tool for studying atomic layer deposition](#)
E Langereis, S B S Heil, H C M Knoops et al.
- [LPCVD against PECVD for micromechanical applications](#)
A Stoffel, A Kovács, W Kronast et al.

Recent citations

- [Measurement of the transmission secondary electron yield of nanometer-thick films in a prototype Timed Photon Counter](#)
T.H.A. van der Reep *et al*



ECS The Electrochemical Society
Advancing solid state & electrochemical science & technology
2021 Virtual Education

Intensive Short Courses


Sun, Oct 10 & Mon, Oct 11

Providing students and professionals with in-depth education on a wide range of topics

Early registration deadline: Sep 13, 2021

Register early and save!

Ultra-thin alumina and silicon nitride MEMS fabricated membranes for the electron multiplication

V Prodanović^{1,2} , H W Chan^{1,2}, H V D Graaf^{2,3} and P M Sarro¹

¹Electronic Components, Technology and Materials (ECTM), Delft University of Technology, Delft, The Netherlands

²National Institute for Subatomic Physics (Nikhef), Amsterdam, The Netherlands

³Delft University of Technology, Delft, The Netherlands

E-mail: v.prodanovic@tudelft.nl

Received 29 October 2017, revised 24 January 2018

Accepted for publication 1 February 2018

Published 22 February 2018



CrossMark

Abstract

In this paper we demonstrate the fabrication of large arrays of ultrathin freestanding membranes (tynodes) for application in a timed photon counter (TiPC), a novel photomultiplier for single electron detection. Low pressure chemical vapour deposited silicon nitride (Si_xN_y) and atomic layer deposited alumina (Al_2O_3) with thicknesses down to only 5 nm are employed for the membrane fabrication. Detailed characterization of structural, mechanical and chemical properties of the utilized films is carried out for different process conditions and thicknesses. Furthermore, the performance of the tynodes is investigated in terms of secondary electron emission, a fundamental attribute that determines their applicability in TiPC. Studied features and presented fabrication methods may be of interest for other MEMS application of alumina and silicon nitride as well, in particular where strong ultra-thin membranes are required.

Keywords: timed photon counter, secondary electron emission, atomic layer deposited alumina, LPCVD silicon nitride, ultra-thin membranes

(Some figures may appear in colour only in the online journal)

Introduction

Timed photon counter (TiPC)

The TiPC is an advanced type of a photodetector for soft photons (energies in the 100–1000 eV range), which has a working principle similar to the photomultiplier tubes (PMTs) [1]. Essential part of TiPC is the tynode (transmission dynode), an array of freestanding membranes with thicknesses in the order of a few nanometers. After the impact of an incoming electron on one side of the tynode, noise-free amplification is provided through secondary electrons emission (SEE) at the opposite side of the membrane. Emission of electrons in transmission mode allows a significant reduction in size and weight of the device in comparison with existing photodetectors. Vertically stacked tynodes put at different potentials in vacuum on top of an all-digital sensing chip

(figure 1), will result in an outstanding performance in terms of spatial and time resolution TiPC can be used in a wide range of applications, including solid state, atomic and molecular physics experiments, medical imaging, and commercial applications such as 3D optical imaging. Moreover, due to the strong electric field between the tynodes, TiPC is expected to be able to operate in the presence of magnetic fields [2, 3].

For the proper operation of the proposed electron multiplier, the tynode material must have a transmission secondary electron yield (TSEY) of 4 or higher, so that no more than five tynodes are utilized for signal detection. Previous studies have often put focus only on reflection configurations, which are of interest for applications such as PMTs, or, in more recent work, microchannel plates (MCPs) [4]. There, a wide range of insulators was reported to have a high reflection SEY (RSEY), which usually suggests efficient electron

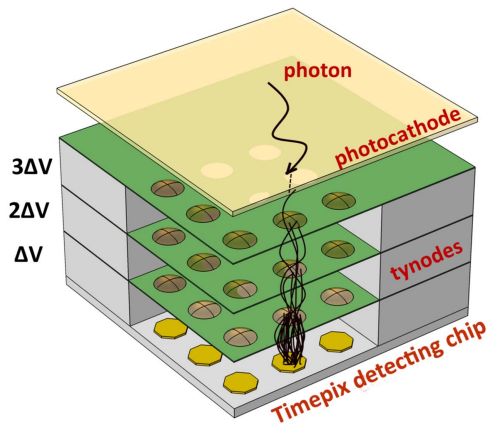


Figure 1. The operating principle of TiPC consists of three steps: 1. Conversion of photon to an electron at a photocathode; 2. Electron multiplication provided by a stack of tynodes with thicknesses of only a few nm; 3. Signal detection through a pixel activation on the TimePix chip.

multiplication in transmission mode as well. However, in transmission mode, some optimal electrical conductivity is required for replenishing vacancies in the membrane after the escape of secondary electrons. To avoid a charge-up effect, the tynodes need to be covered by a very thin electrically conductive layer. Another vital requirement relates to the mechanical and chemical properties of the selected tynode material. Low residual stress and chemical inertness to certain etchants used in MEMS technologies are desired, as the membrane material must be mechanically and chemically stable during and after the fabrication process.

Low pressure chemical vapour deposition (LPCVD) silicon nitride

LPCVD is a standard high-throughput technique for the growth of conformal and uniform Si_xN_y films at pressures below 1 Torr. Thin silicon nitride films grown by this method are very frequently used in the IC industry as passivation layers, or as masking layer for selective oxidation and for KOH etching. As Si-rich Si_xN_y has shown to have a low residual stress [5], it is an attractive material for the manufacturing of strong ultra-thin membranes. Such transparent windows with thicknesses down to 15 nm have been used, among others, for *in situ* electron microscopy [6, 7].

ALD alumina

Atomic layer deposition (ALD) is a gas-phase method for growing ultrathin films based on sequential self-limiting surface reactions. Precise thickness control over a large area and conformal covering of high aspect ratio structures with continuous, pinhole-free, films are among the outstanding merits of this technology [8, 9]. Moreover, ALD is suitable for coating a wide range of substrates, including thermally sensitive materials, such as polymers, as it can be performed at low temperatures, even at room temperature [10, 11]. Numerous high quality metallic and ceramic ALD films have been applied in nanotechnology, photovoltaics, organic and

flexible electronics. New areas where ALD may be employed are emerging very fast, due to the continuous requirement for scaling down of devices in microelectronics.

The growth of Al_2O_3 is one of the most extensively studied ALD processes. Being a high- k material with excellent dielectric properties, it has a great potential to replace SiO_2 as a gate dielectric. ALD alumina is known to be thermally and chemically stable, with a good adhesion to many surfaces in a wide temperature range [10, 12]. Furthermore, it is applied as a passivation, buffer and barrier layer in the photovoltaic industry [13], and also as a coating for corrosion protection [14]. In MEMS processing a very thin alumina can be used as extremely efficient masking material during a deep reactive ion Si etching at cryogenic temperatures [15]. With regard to the photomultiplier research field, ALD alumina films are used to tailor the resistance and SEE properties of large-area borosilicate glass capillary arrays for MCP based detectors with a high gain and low noise. Optimization of ALD processes for this application gave the maximum RSEY value of around 3 [4].

Due to its mechanical strength and low residual stress [16], ALD alumina is a very attractive material for the fabrication of large suspended membranes. Moreover, its chemical stability towards common dry etching procedures is of great importance during the release of membranes. Nanocorrugated suspended alumina membranes have been fabricated on top of Si nanograss and a monolayer of self-aligned polymeric nanobeads [17]. Recently a formation of large freestanding 25 nm thin ALD alumina plates are reported [18]. This material is robust, stiff, ultra-lightweight and has the ability to 'pop-back' to its original shape without damage after sharp bends.

Fabrication of tynodes

In this section we introduce the process developed for the fabrication of tynodes using (LPCVD) silicon nitride and (ALD) alumina, schematically depicted in figure 2. Substrates used in both processes are single side polished 4 inch (100), phosphorus doped ($5\text{--}10\ \Omega\ \text{cm}$) wafers with thicknesses of $(500 \pm 15)\ \mu\text{m}$. Prior to the processing, the wafers are subjected to a standard cleaning procedure including 10 min long dip in 99% ('fuming') and 69% ('boiling') HNO_3 , each followed by rinsing in de-ionized H_2O . After that, the Si substrate is oxidized in a wet thermal environment at $1000\ ^\circ\text{C}$, for a resulting oxide thickness of 300 nm. Moving further, a 500 nm thick optimized low-stress LPCVD silicon nitride layer is deposited to serve as a support material in which tynodes are suspended (top image on figure 2). This film is then patterned on the front side of the wafers, using hexafluoroethane (C_2F_6) etching chemistry to form the tynode grid. These wells, which will later define the geometry of the tynodes, are designed to have a diameter ranging from 10 to $30\ \mu\text{m}$, whereas the total size of the array goes up to 128×128 tynodes, with a centre-to-centre pitch of $55\ \mu\text{m}$. After the described template is prepared, the flowcharts for the two chosen tynode materials resume along different directions.

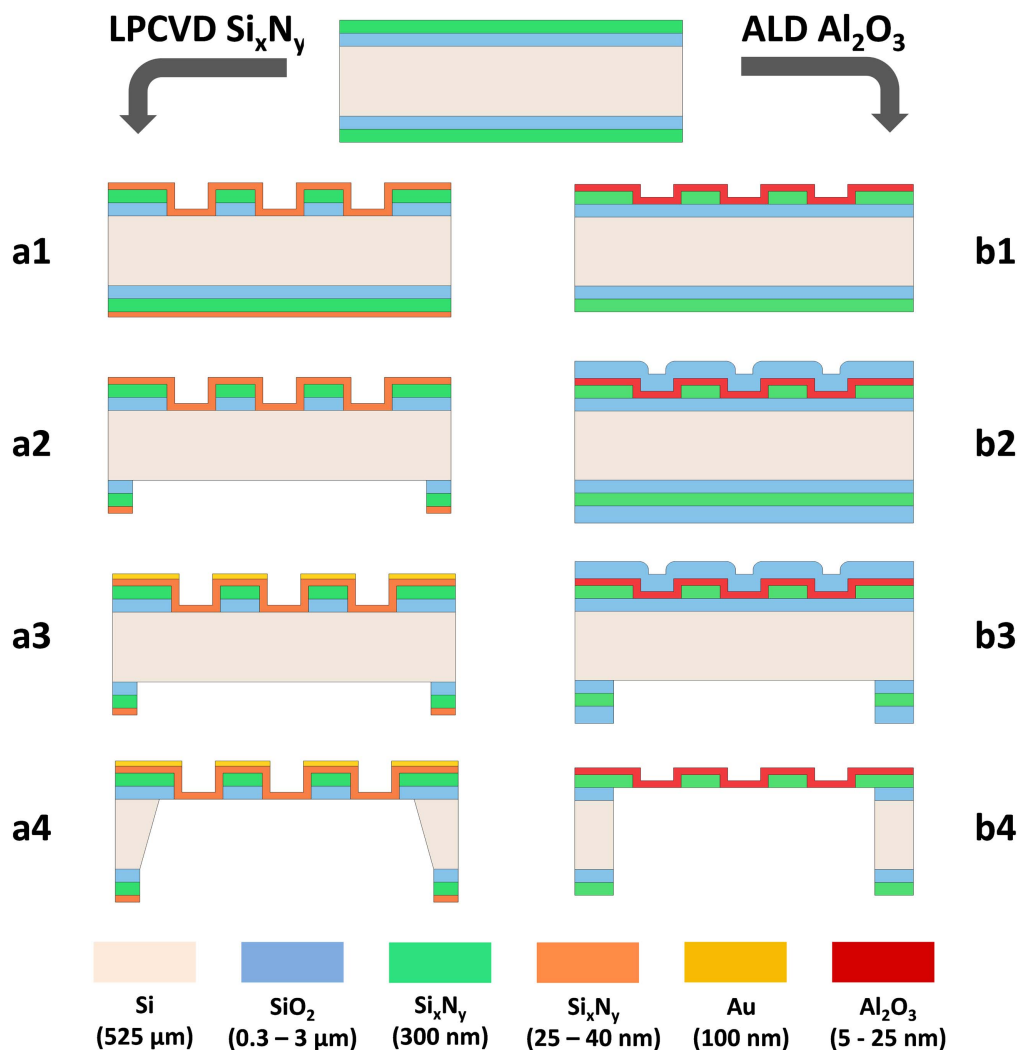


Figure 2. MEMS fabrication flowchart of the tynodes, with on the left the procedure for LPCVD silicon nitride and on the right for the ALD alumina as the tynode material.

LPCVD silicon nitride. The thin oxide film left after the dry etching step is subsequently removed in a 5% HF solution. This is performed as a precaution step to ensure that the membrane material is deposited on a smoothed surface without sharp corners. Then, the Si_xN_y was deposited in a horizontal LPCVD Tempress Systems reactor (figure 2(a1)). Wafers were loaded in a vertical position in slits of a quartz boat. Ultra-pure nitrogen was used for pressure control and purging during the loading. We used the most typical gas mixture for this LPCVD process, namely dichlorosilane (SiH_2Cl_2 , DCS) and ammonia (NH_3). The amount of gasses flowing in the tube was regulated by flow meters that allow a maximum flow of 500 sccm (in this work the total gas flow was, however, set to 400 sccm). Deposition temperature and pressure were set to 850 °C and 150 mTorr, respectively.

For the investigation of the SEY of Si_xN_y , we fabricated four types of tynodes with two different thicknesses, namely 25 and 40 nm. Next, the Si content in the films was increased by tuning DCS/ammonia mixture ratio to 5.67 ('Type 1' Si_xN_y film) and to 9 ('Type 2' Si_xN_y film), while the total gas flow was kept constant. The tuning of process parameters was

aiming at lowering the layer resistivity, driven by the need to suppress the charge up effects occurring in the setup for the SEE analysis. After deposition of the tynode material, large windows on the backside of wafers are etched (figure 2(a2)). As a conductive film in between membranes, we used 100 nm thin evaporated gold on 10 nm of Cr, patterned by a lift-off technique (figure 2(a3)). Then, the wafers were mechanically sawed into $2 \times 2 \text{ cm}^2$ chips, in order to avoid dicing after release of the tynodes. Etching of Si substrate was attained by 33% KOH continuously stirred solution, at the temperature of 85 °C. Both Si_xN_y and Au are inert to the employed etchant and for this reason no protective vacuum holder is required for the final release of the membranes (figure 2(a4)). A wash in 5% HCl solution followed by a dip in 99% HNO_3 , each 15 min long, proved to be efficient in the final cleaning procedure of samples and removal of, most likely, iron oxide particles present in the KOH bath. Finally, samples were rinsed by a gentle flow of DI water and dried in air. scanning electron microscope (SEM) image of one of fabricated tynode is shown on figure 3(a).

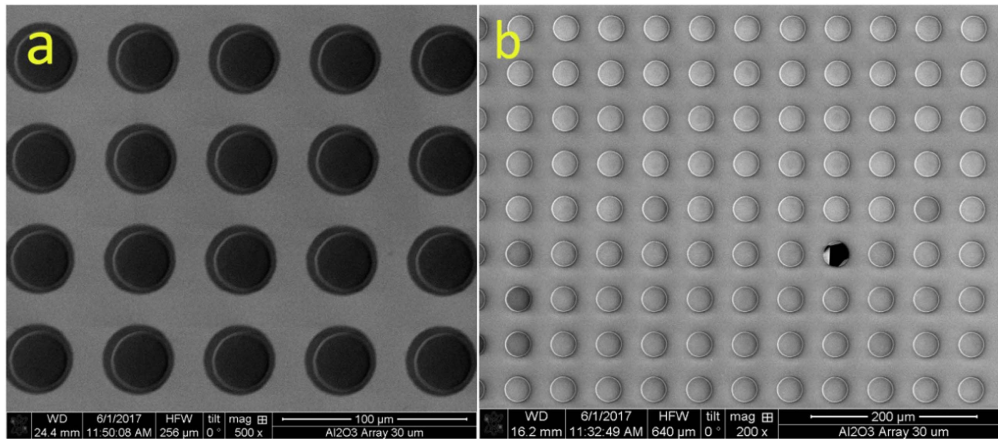


Figure 3. SEM images of a 25 nm thin ‘Type 2’ Si_3N_4 (a) and 15 nm thin alumina (b) tynodes with a diameter of 30 μm . Total size of array is 64×64 membranes with a pitch of 55 μm . SEM inspection revealed that the largest number of membranes remained intact after the release.

ALD alumina. For the growth of alumina films we used a thermal ALD ASM F-120 reactor where trimethyl-aluminium (TMA) and water are employed as aluminium and oxygen source, respectively. This deposition method is widely studied and mapped out for different substrates in other reports [16, 19, 20]. Upon the introduction to a deposition chamber, TMA easily reacts with hydroxyl groups on the surface. After this reaction is completed, the excess of precursor and by-products are purged away by nitrogen. The same process is then repeated for water, which reacts with methyl sites. As a result, no mixing of two precursors occurs in the gas phase, which eliminates incorporation of particles in the ALD film. In each cycle one (sub)monolayer of Al_2O_3 is grown. One ALD cycle is accomplished in a sequence 1 s–6 s–1 s–6 s long steps, corresponding to pulsing time of TMA, N_2 , H_2O and N_2 , respectively. The film growth is carried out at the pressure of 1 Torr, whereas the temperature was kept at 300 °C. The number of cycles is varied from 55 to 250, for the deposition of layers with thicknesses from of 5 to 25 nm, respectively. It is important to note that alumina growth in the valleys of the grid is performed on intentionally left thermal oxide (figure 2(b1)). In order to avoid any possible thinning down or degradation of the very thin alumina films during remaining processing steps, the alumina layer was capped with 1 μm of PECVD oxide (figure 2(b2)). Large windows on the backside of the wafers were then opened by etching the silicon substrate in a deep reactive ion etching process, with 3 μm thick PECVD oxide as a hard mask material (figure 2(b3)). In parallel, additional lines are etched to facilitate manual dicing of the wafers into $2 \times 2 \text{ cm}^2$ large chips. Final release of the tynodes was carried out by removing the sacrificial oxide layers in an HF vapour chamber (figure 2(b4)). For the removal of the oxide layer on both sides of alumina we applied 4 to 5 etching cycles, each 10 min long, at 125 Torr, with steps for chamber purging in between. Flows of HF and ethanol were 190 sccm and 210 sccm, respectively. For these conditions, calculated selectivity between thermal and PECVD oxide was 1:35. On the contrary, alumina is known for being an excellent protective layer during HV vapour etching. To prove this, a

wafer with 5 nm thin ALD alumina film deposited on top of 100 nm thermal oxide was exposed to 60 min long etching, after which no change in the thickness or pinholes were observed. Figure 3(b) shows an SEM capture of a 15 nm thin alumina tynode after the release and sputtering of 2 nm TiN as a required conductive layer.

Characterization techniques

The mechanical, structural and electrical properties of LPCVD silicon nitride and ALD alumina films used for the tynodes fabrication are investigated. Stress values are determined by measuring the wafer curvature prior and after the deposition of the film under investigation (TENCOR FLX-2908 Silecs), using the well-known Stoney formula given elsewhere [21]. Thickness and refractive index of the films were determined by variable angle spectroscopic ellipsometry. The employed instrument was visible and near-infrared extended Woollam M200UI (245–1700 nm). The thicknesses of silicon nitride and alumina films were extracted using a Cauchy dispersion model. In order to check the uniformity of the layer, we recorded data in 13 points across the wafers. X-ray photoelectron spectroscopy (XPS) is employed for the composition analysis. Wide scans were acquired using 200 eV analyser pass energy and a 1 eV step. High resolution spectra of the Al 2p and O 1s regions were recorded using 50 eV pass energy and 0.1 eV steps. Information on surface roughness is obtained by atomic force microscopy (AFM) in a noncontact mode, with a silicon tip (radius 5 nm), over $0.5 \times 0.5 \mu\text{m}^2$ or $2 \times 2 \mu\text{m}^2$ large area. For the TSEY analysis of the Tynodes a special setup is built that can be mounted onto the stage of a SEM (NovaNanoLab 650 Dual Beam). It consists of a sample holder, a retarding grid and a collector insulated from each other. They are connected to Keithley 2450 sourcemeters via a feedthrough allowing bias potentials of -200 to 200 V to be used while measuring the current simultaneously. This allows true secondary electrons (with energies lower than 50 eV) to be separated from back-scattered electrons. The imaging capabilities of the SEM is used to locate and direct the electron beam onto the tynodes.

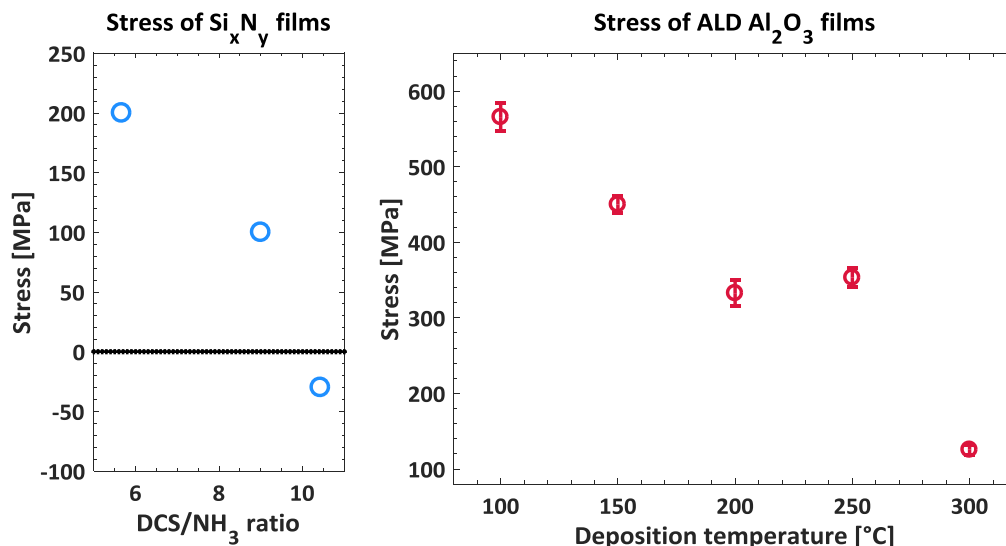


Figure 4. Stress of LPCVD Si_xN_y (left) and ALD Al₂O₃ (right) films prepared at different process conditions. Stress is investigated for silicon nitride films with thickness of around 1000 nm (with deposition times between 140 and 162 min), whereas alumina was approximately 100 nm thick (1000 cycles long ALD runs). Vertical bars represent a standard deviation calculated out of five subsequent stress measurements for each wafer.

The electron beam energy ranges from 0.3 to 30 keV with an electron beam current of a few pA to a few nA.

Results and discussion

In the following section the tynode materials performance, in relation to the properties of interest for TiPC and other possible MEMS applications, is compared and discussed. In an attempt to reduce charge up effects after the escape of secondary electrons from the tynode film, we developed Si_xN_y layers with a higher Si amount. This was achieved by controlling the composition of the gas mixture in the LPCVD process. In the envisioned further optimization of the TiPC operation, focusing of secondary electrons along the stack of the tynodes is a desirable capability. This can be achieved using lens-shaped tynodes, which could be fabricated using reflowed photoresist as a substrate for the growth of the tynode material. This requires a low temperature deposition process of the tynode material. Such a demand cannot be met by LPCVD, but the nature of ALD, in contrast, allows forming films of a high quality even at a room temperature. With this aim, attributes of ALD alumina grown at temperatures of down to 100 °C were explored. In addition, the thickness of the tynodes is as it is one of the key factors in the secondary electron emission.

Residual stress

We evaluated the stress of alumina films grown during 1000 cycles in the temperature range from 100 °C to 300 °C (figure 4, left plot). Longer depositions are performed for this investigation in order to avoid measurement error which arises for very thin layers. The film present on the back side of the wafer was removed prior to the curvature measurement, either in BHF solution while the front side was protected with

photoresist, or by a dry etching method using boron trichloride (BCl₃), in the case of deposition temperature of 150 °C, due to the unavailability of some cleanroom facilities at the time this process was performed. It was observed that tensile stress gradually increased from 125 to 565 MPa for decreasing temperature in the investigated domain. This result is in line with other reports on thermo-mechanical properties of ALD alumina [16, 22, 23]. In parallel, we noticed a larger fluctuation of repeated measurements at lower deposition temperatures, with an exception for films grown at 150 °C. This may suggest that a temporary presence of a photoresist on top of ALD alumina during etching on the backside influences its residual stress. Left plot on figure 4 reveals that LPCVD Si_xN_y has even lower tensile stress with a possibility of conversion to compressive values if Si content is sufficiently enhanced [24]. Having this aspect in mind, we conclude that ALD alumina is a more advantageous choice than LPCVD Si_xN_y for the MEMS fabrication of tynodes, as stress of the same magnitude is obtained at significantly lower deposition temperatures. The change of stress caused by sputtering of TiN is investigated on non-patterned alumina films deposited at 300 °C. Presence of 2 nm thin TiN on top of 100 nm alumina film decreased the stress for approximately 50 MPa. Since much thinner alumina was used for the fabrication of tynodes, the same effect is investigated for the combination of 5 nm alumina covered with 2 nm of TiN. Here the induced change of stress was much larger: initial stress of 243 ± 32 MPa dropped to tensile values of -225 ± 39 MPa. The stress of TiN alone was found to be -1.7 ± 0.1 GPa. However, sputtering of TiN even on the thinnest alumina tynodes did not cause noticeable cracking within the array.

Thickness and optical properties

The thickness and refractive index of Si_xN_y layers grown on top of Si substrate in a 15 min long deposition process, while

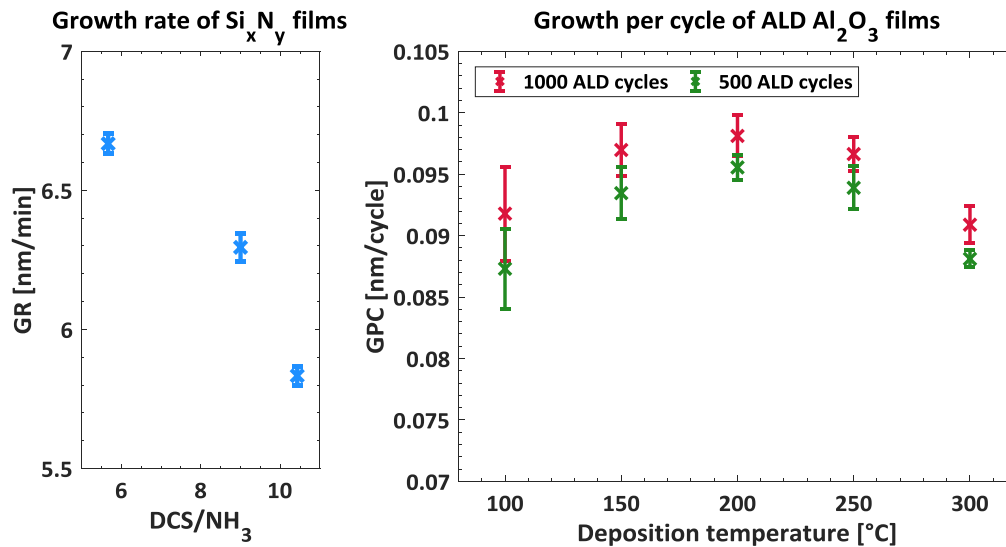


Figure 5. Growth rate of Si_xN_y layers for different DCS/ammonia ratio in the 15 min long LPCVD process (Left graph). Plot on the right side shows average thickness of ALD alumina obtained per cycle in the temperature range 100 °C–300 °C (left plot). Films were grown during 500 (green markers) and 1000 (red markers) ALD cycles. Vertical bars represent standard deviation in GPC, calculated from 13 data points across 4 inch wafers.

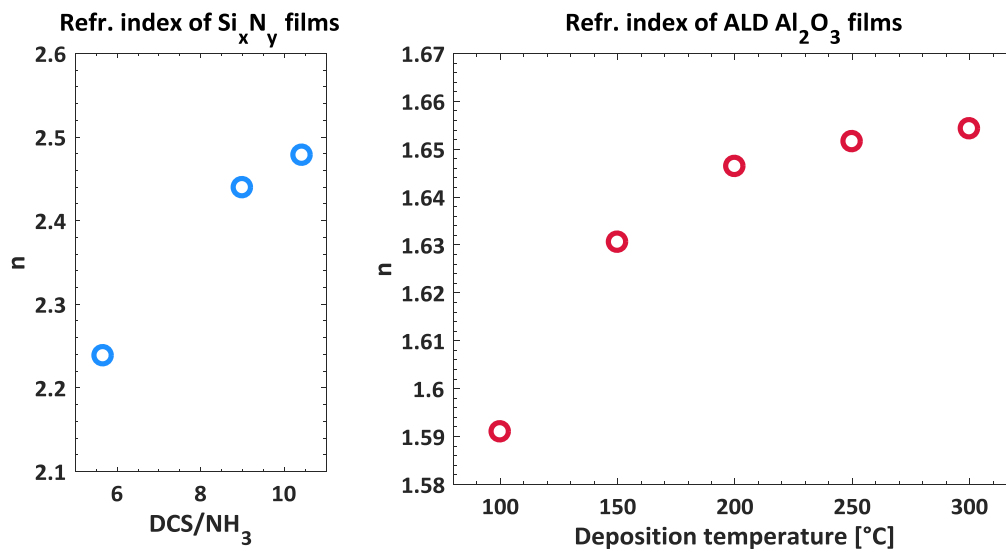


Figure 6. Refractive index of LPCVD Si_xN_y (left) and ALD alumina (right) at the wavelength of 633 nm. Alumina films were grown in 1000 ALD cycles long processes, whereas the Si_xN_y deposition time was set to 15 min, so that all layers were approximately 100 nm thin.

using different flows of gasses, was studied. As shown on figure 5 (left), the growth rate (GR) of Si_xN_y films reduces with the increase of DCS/ NH_3 ratio. The most efficient employed gas mixture, containing 340 sccm NH_3 and 60 sccm of DCS, resulted in a deposition rate of 6.67 nm min^{-1} , whereas somewhat slower growth (5.83 nm min^{-1}) was noted for the highest investigated flow of DCS (DCS/ $\text{NH}_3 = 365/35$). All films exhibit very good thickness uniformity, with standard deviations in the range of only 0.51–0.76 nm measured in 13 points across (4 inch) wafers. Left plot on figure 6 shows the significant influence of gas composition on the refractive index. Namely, higher flow of DCS caused the elevation of refractive index from 2.23 to 2.47, which indicates a higher Si content in the material.

The growth per cycle (GPC) of ALD alumina in the temperature range 100 °C–300 °C is plotted in figure 5 (right). We evaluated films deposited on top of silicon and calculated GPC as average thickness divided by total number of cycles, which was set to 500 and 1000. An apex in the profile of GPC observed at 200 °C is in accordance with previous studies [25–29], which showed that at higher temperatures, due to the decrease of OH sites (dehydroxylation) on the surface, the growth is slowed down. At lower temperatures, on the other hand, mass transport drops and reactions between precursor gasses and surface become incomplete. Clearly, films deposited at higher temperatures have better uniformity, with standard deviation of only 0.347 nm measured after 500 cycles long deposition at 300 °C. Large variations of

Table 1. Overview of literature results on growth per cycle and refractive index of ALD alumina films prepared at different temperatures.

Number of cycles	GPC (nm/cycle)	Refr. index	Dep. temp. (°C)	References
2730	0.11	1.666	300	[8]
/	0.09	/	220	[15]
800	0.14	1.61–1.66	150	[26]
/	0.15	1.63–1.69	175	
/	0.08	/	100	[27]
/	0.10		200	
/	0.09		300	
/	0.09	1.60	100	[28]
/	0.11	1.63	200	
/	0.10	1.64	300	
/	0.08	1.64	200	[29]
1000	0.091	1.654	300	This work
	0.097	1.652	250	
	0.098	1.646	200	
	0.097	1.631	150	
	0.092	1.591	100	

thickness in the process conducted at temperatures lower than 150 °C suggest that purging times should be longer than 6 s. Investigated GPC values are very close to or slightly lower than deposition processes reported elsewhere (see table 1).

Deposition temperatures close to 200 °C provide the fastest growth, in agreement with all other studies on ALD of alumina with similar process parameters. Higher values of GPC obtained for longer depositions (1000 cycles) indicate a delay of a homogeneous growth. This incubation period is difficult to be evaluated by *ex situ* ellipsometry analysis. Also, it should be discerned that native oxide was not taken into account, hence the true thickness of ALD alumina is somewhat lower for the observed growth on Si substrate. In study by Groner *et al* [10] around 0.2 nm of interfacial SiO₂ was determined to be present in between Si and alumina.

The effect of deposition temperature on the refractive index at 633 nm is shown on figure 6 (right). Refractive index has the value of around 1.65 at 300 °C and it drops with the decrease of temperature. Its sharper reduction at temperatures below 200 °C may be caused by presence of carbon and hydrogen impurities in these films, as suggested in [16].

Elemental composition

For the evaluation of elemental composition of deposited films, we performed XPS measurements on the surface of samples (not presented here), but also in-depth profiling by ion beam etching to eliminate the contribution of surface impurities. Al₂O₃ with thicknesses of around 100 and 40 nm thin Si_xN_y, both on top of Si substrate, were used for this characterization. From a high resolution acquisition around Si2p and N1s peaks we calculated atomic percentage of silicon to be only slightly higher for a film with grown with a DCS/ammonia ratio of 9 (table 2). Namely, nitrogen to

silicon ratio was determined to reduce from 1.03 to 1 after the flow of ammonia in the gas mixture was decreased by 20 sccm, and that of DCS increased by the same amount. Oxygen portion in the bulk is found to be around 4.5% for both films. In contrast, it increases to 20.5% on the surface, which implies a strong oxidation (figure 7). However, it should be emphasized that samples were not subjected to any cleaning procedure prior to the XPS investigation.

XPS spectrum in the bulk of alumina films reveals the presence of aluminium and oxygen, as expected. Since carbon (C1s) peak was not detected in all of the prepared samples, we will analyse data normalization of XPS plots. Zoom-in of Al2p region indicates symmetry in the shape of these peaks, but with a drop in the intensity of the film prepared at 100 °C, suggesting a somewhat lower aluminium amount. On the other hand, we observed broadening and displacement towards lower energies for O1s peaks attributed to temperatures of 150 °C and 100 °C, which indicates the presence of hydroxyl and/or carbon related bonds in the material. This observation is in line with other reports on similarly conditioned ALD processes [26, 29]. Nevertheless, materials prepared at temperatures in the range 150 °C–300 °C display a good stoichiometry, with in-bulk oxygen to aluminium elemental ratio of 1.49–1.50. We determined this parameter from the narrow XPS acquisition around Al2p and O1s peaks and proved that the molecular formula of investigated material is indeed Al₂O₃. On the other hand, O:Al ratio elevated to 1.60 for the growth temperature of 100 °C (figure 8). Moreover, this is the only film that revealed the incorporation of carbon, which also affected the profile of its O1s peak (table 2).

Surface morphology. AFM analysis of LPCVD Si_xN_y shows that the surface of these films is very smooth, uniform and without hillocks formation. We observed a negligible increase of surface roughness when a gas mixture with a higher DCS content is employed, as shown in figures 9(a), (b). Similarly, scanning over 0.5 × 0.5 μm² area of alumina samples reveals that lowering the deposition temperature does not affect the surface morphology. Average roughness (RMS) of a film prepared at 100 °C is only 0.05 nm higher than the layer formed during the same number of reaction cycles at 300 °C (figures 9(c), (d)). Such superb smoothness with RMS of 0.25 nm is even lower than previous investigations where it was reported to be between 0.5 and 2 nm [10, 12]. Amorphous structure of silicon nitride and alumina films was not confirmed by XRD analysis in this work, but according to other studies crystallization of Al₂O₃ occurs only during thermal annealing at temperatures higher of around 900 °C [30]. Silicon nitride, on the other hand, exhibited no crystallographic peaks even after the bake-out procedures at temperatures of up to 1000 °C [5]. AFM investigation discloses adequacy of both alumina and silicon nitride for the fabrication of smooth tynodes for the TiPC application. Furthermore, we observed that the previously described

Table 2. Information on relevant peaks and atomic content of the studied films, obtained from in-depth XPS survey. The remaining portion, usually around 1.45%, originates from Ar used in the ion beam etching of the material. For this characterization we used alumina films deposited during 1000 cycles and 40 nm thin Si_xN_y , both on top of Si substrate. Since carbon was not present in all of prepared samples, plots were not normalized to C1s or any other peak.

Si_xN_y						
DCS/ammonia	Si2p (%)	N1s(%)	O1s (%)	Peak position/FWHM (eV)		
				Si2p	N1s	O1s
5.67	46.21	47.85	4.53	102.12/2.88	398.10/2.55	532.49/1.63
9	47.21	46.88	4.45	102.10/2.95	398.15/2.52	532.83/2.70
Al_2O_3						
Deposition temperature (°C)	Al2p (%)	O1s (%)	C1s (%)	Peak position/FWHM (eV)		
				Al2p	O1s	C1s
100	37.04	59.48	1.51	76.77/2.82	533.16/3.42	285.07/3.79
150	39.42	59.11	/	76.78/1.79	532.98/3.16	/
200	39.38	58.52	/	76.85/2.65	533.29/2.79	/
250	39.55	58.95	/	76.83/2.64	533.24/2.82	/
300	39.54	59.05	/	76.83/2.67	533.21/2.88	/

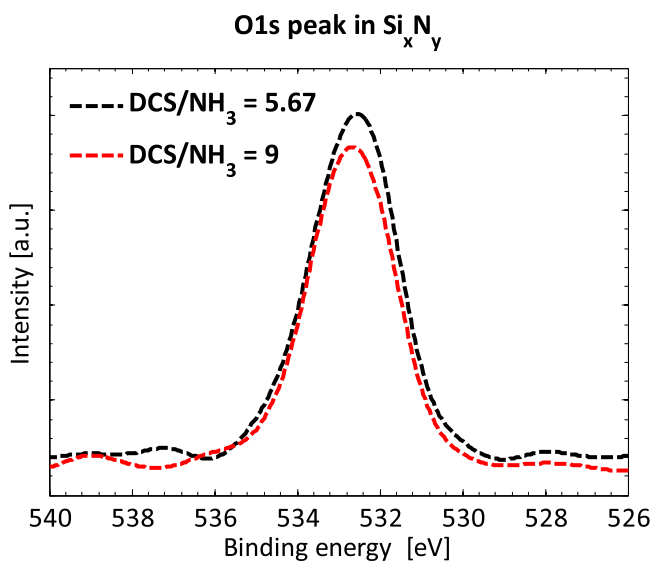


Figure 7. In-bulk XPS spectra of O1s peaks in Si_xN_y layers.

adjustment of deposition parameters has a marginal influence on surface roughness.

Secondary electron emission. Primary electrons traversing through the tynode material interact with it and lose energy. In this process, secondary electrons which can escape from the reflection or transmission side are generated. Their emission coefficients are given by SEY and TSEY, respectively. Apart from the low-energetic secondary electrons (<50 eV), there are also high-energetic (>50 eV), backscattered and forward scattered electrons. Their emission coefficient are BSEY and FSEY, respectively. The low- and high energetic electrons can be separated by using a

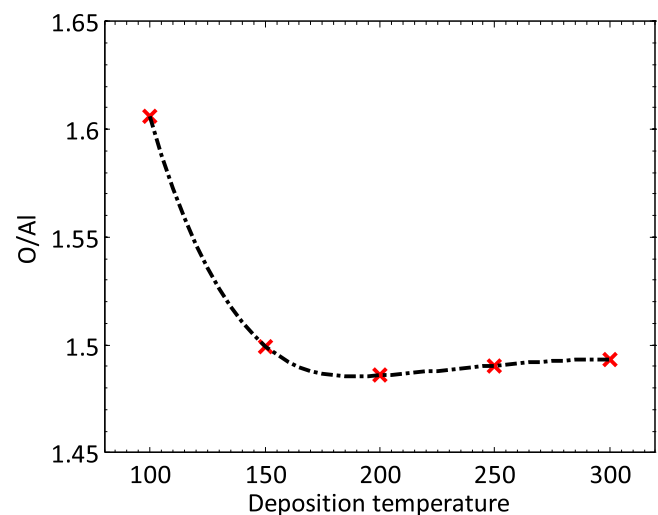


Figure 8. Oxygen-to-aluminium atomic ratio in ALD alumina films. Values are calculated using the total surface under Al2p and O1s peaks, including the contribution of C–O bonds for deposition temperature of 100 °C.

negatively and positively biased sample. At first, the total transmission yield (TEY) and total reflection yield (REY) that contains both type of electrons are measured. In the second measurement, the positively biased sample retracts the low-energetic electrons, so only the BSEY and the FSEY are measured. By subtracting values of these two measurements, the two measurements yields the true secondary electron emission is obtained.

These currents were measured on 40 nm thin Si_xN_y tynodes with two different DCS/ NH_3 ratios: 5.67 ('Type 1') and 9 ('Type 2'), as plotted on figure 10. Energy of primary electrons in the SEM was increased from 0.3 to 10 keV, with

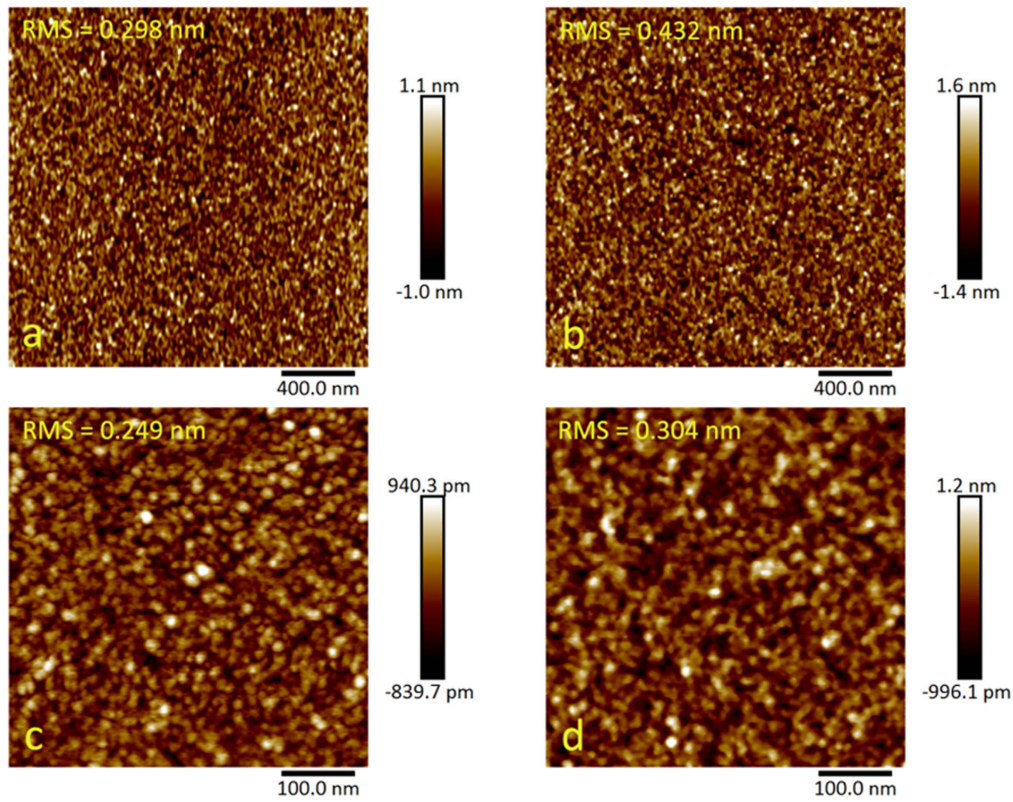


Figure 9. AFM analysis of investigated materials: a $2 \times 2 \mu\text{m}^2$ large area of 40 nm thin silicon nitride deposited using gas mixture with DCS: NH_3 ratio of 5.67 (a) and 10.43 (b). Lower micrographs are recorded over $0.5 \times 0.5 \mu\text{m}^2$ region of 50 nm thin ALD alumina layers grown at 300 °C (c) and 100 °C (d). All films were deposited on top of a Si substrate.

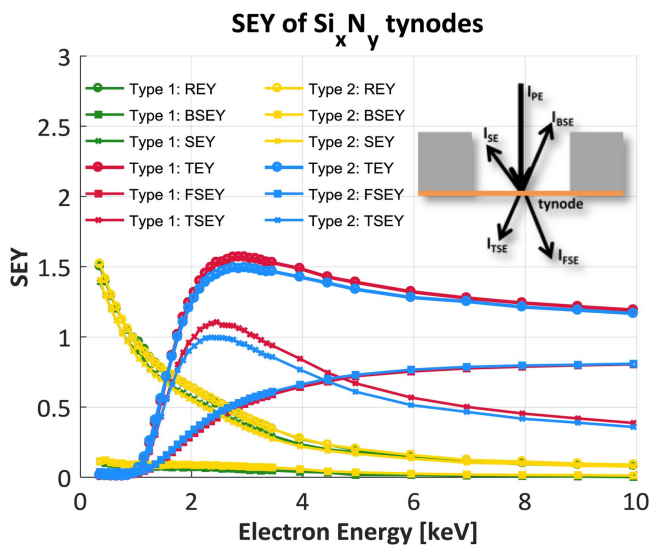


Figure 10. Electron emission coefficients of 40 nm thin Si_xN_y tynodes. ‘Type 1’ and ‘Type 2’ stand for Si_xN_y films deposited by using DCS/ NH_3 ratio of 5.67 and 9, respectively. Inserted image in the upper right corner shows currents used for calculations of electron emission coefficients of tynodes.

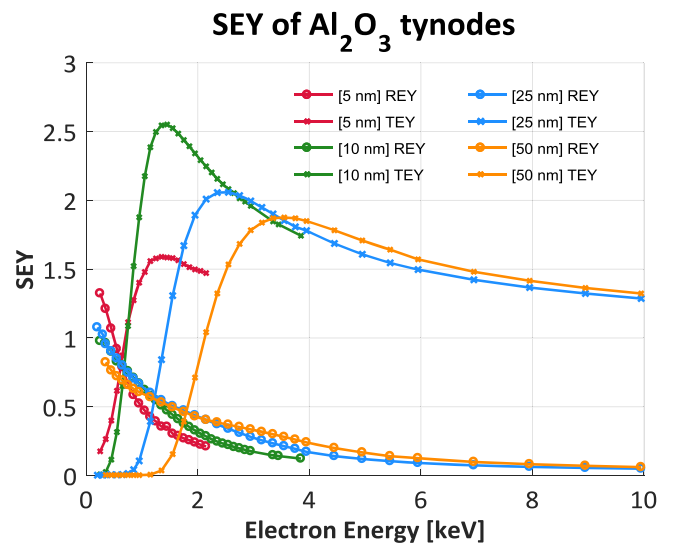


Figure 11. Reflection (REY) and transmission (TEY) secondary electron coefficients of ALD alumina tynodes with thicknesses in the range from 5 to 50 nm. A conductive 5 nm TiN film was sputtered on the backside of membranes to prevent charging up.

coarse steps in the tail of the curves. For the elimination of charge up effects, around 2 nm of TiN was sputtered on the backside of the membranes prior to this investigation. A slightly better response is observed for the tynode ‘Type 1’,

with a maximum TSEY of 1.57 corresponding to the energy of 2.85 keV. TSEY peak of 1.49 occurred at the same position for the ‘Type 2’ sample, which proves that thicknesses of these two tynodes are indeed identical.

ALD alumina tynodes with thicknesses in the range 5–50 nm were subjected to identical characterization. Outcome of this analysis is presented in figure 11 and includes only total yields (REY and TEY). The survey showed that TiPC may benefit more from the alumina as material than the previously investigated Si_xN_y . The most suitable sample, 10 nm thin alumina tynode, exhibits TEY of 2.6. Moreover, these samples are more sensitive at lower energies, which is of a great importance for our application. Next, we detected that TSEY peak drops and shifts towards higher energies for the thicker alumina tynodes. Still, even 50 nm thick alumina membranes are a more efficient secondary electron emitter than silicon nitride samples with thicknesses of 40 nm. The lower yield obtained for 5 nm thin alumina tynode suggests that the decrease in interaction volume of the primary electrons with the tynode leads to a decrease in the number of generated secondary electrons. In transmission mode, there is an optimum thickness for which the largest number of secondary electrons are generated within the escape depth of the material.

Conclusions

This study explores applicability of LPCVD Si_xN_y and ALD Al_2O_3 as tynode materials in TiPC. Mechanical and structural properties of these films showed that they are both qualified for the fabrication of strong, homogenous membranes. Investigated materials exhibit very low stress tensile, high uniformity in thickness, absence of impurities and remarkably smooth surface. However, the ALD method proved to have two outstanding advantages—it allows formation of high quality films that are even thinner than those obtained with LPCVD procedure, and at much lower temperatures. Thinner tynodes are required for the detection of low energetic photoelectrons in the TiPC, whereas the low-temperature deposition is generally desired since they provide higher degree of freedom in MEMS processing. Finally, with a dedicated multi-electrode setup in SEM, we demonstrated that alumina is a more efficient secondary electron emitter, with a TSEY of 2.6 for the 10 nm thin tynode, in contrast to the value of around 1.6 obtained for 40 nm thin silicon nitride tynode. Further improvement of SEY can be achieved by investigating proper surface termination which may introduce negative electron affinity, *in situ* surface cleaning of tynodes during the measurement procedure, and by adjusting the shape of the membranes for secondary electrons focusing.

Acknowledgments

Authors would like to express their gratitude to technical staff at Else Kooi Laboratory which provided support in the fabrication process of tynodes.

ORCID iDs

V Prodanović  <https://orcid.org/0000-0002-9206-0136>

References

- [1] Hamamatsu Photonics 2006 *Photomultiplier Tubes: Basics and Applications* (Iwata City, Japan: Hamamatsu Photonics K.K.)
- [2] van der Graaf H *et al* 2017 The tynode: a new vacuum electron multiplier *Nucl. Instrum. Methods Phys. Res. A* **847** 148–61
- [3] Van Der Graaf H *et al* 2013 The Topsy single soft photon detector and the Trixy ultrafast tracking detector *J. Instrum.* **8** 1–7
- [4] Mane A U *et al* 2012 An atomic layer deposition method to fabricate economical and robust large area microchannel plates for photodetectors *Phys. Proc.* **37** 722–32
- [5] French P J, Sarro P M, Mallee R, Fakkeldij E J M and Wolffenbittel R F 1997 Optimization of a low-stress silicon nitride process for surface-micromachining applications *Sensors Actuators A* **58** 149–57
- [6] Alan T *et al* 2012 Micro-fabricated channel with ultra-thin yet ultra-strong windows enables electron microscopy under 4 bar pressure *Appl. Phys. Lett. Rev. Sci. Instrum.* **100** 1–4
- [7] Ramachandra R, Demers H and De Jonge N 2011 Atomic-resolution scanning transmission electron microscopy through 50 nm thick silicon nitride membranes *Appl. Phys. Lett.* **98** 1–3
- [8] Ritala M, Leskelä M, Dekker J, Mutsaers C, Soininen P J and Skarp J 1999 Perfectly conformal TiN and Al_2O_3 films deposited by atomic layer deposition *Chem. Vapor Depos.* **5** 7–9
- [9] Grigoras K, Airaksinen V-M and Franssila S 2009 Coating of nanoporous membranes: atomic layer deposition versus sputtering *J. Nanosci. Nanotechnol.* **9** 3763–70
- [10] Groner M D, Fabreguette F H, Elam J W and George S M 2004 Low-temperature Al_2O_3 atomic layer deposition *Chem. Mater.* **16** 639–45
- [11] Niskanen A, Arstila K, Ritala M and Leskelä M 2005 Low-temperature deposition of aluminum oxide by radical enhanced atomic layer deposition *J. Electrochem. Soc.* **152** F90–3
- [12] Groner M D, Elam J W, Fabreguette F H and George S M 2002 Electrical characterization of thin Al_2O_3 films grown by atomic layer deposition on silicon and various metal substrates *Thin Solid Films* **413** 186–97
- [13] Van Delft J A, Garcia-Alonso D and Kessels W M M 2012 Atomic layer deposition for photovoltaics: applications and prospects for solar cell manufacturing *Semicond. Sci. Technol.* **27** 7
- [14] Potts S E *et al* 2011 Ultra-thin aluminium oxide films deposited by plasma-enhanced atomic layer deposition for corrosion protection *J. Electrochem. Soc.* **158** C132–8
- [15] Grigoras K, Sainiemi L, Tiilikainen J, Säynätjoki A, Airaksinen V M and Franssila S 2007 Application of ultra-thin aluminum oxide etch mask made by atomic layer deposition technique *J. Phys.: Conf. Ser.* **61** 369–73
- [16] Ylivaara O M E *et al* 2014 Aluminum oxide from trimethylaluminum and water by atomic layer deposition: the temperature dependence of residual stress, elastic modulus, hardness and adhesion *Thin Solid Films* **552** 124–35
- [17] Sainiemi L, Grigoras K and Franssila S 2009 Suspended nanostructured alumina membranes *Nanotechnology* **20** 1–6
- [18] Davami K *et al* 2015 Ultralight shape-recovering plate mechanical metamaterials *Nat. Commun.* **6** 1–7
- [19] Nguyen H M T, Tang H-Y, Huang W-F and Lin M C 2014 Mechanisms for reactions of trimethylaluminum with molecular oxygen and water *Comput. Theor. Chem.* **1035** 39–43
- [20] Dillon A C, Ott A W, Way J D and George S M 1995 Surface chemistry of Al_2O_3 deposition using $\text{Al}(\text{CH}_3)_3$ and H_2O in a binary reaction sequence *Surf. Sci.* **322** 230–42
- [21] Stoney G G 1909 The tensions of metallic films deposited by electrolysis *Proc. R. Soc.* **82** 172–5

- [22] Tripp M K *et al* 2006 The mechanical properties of atomic layer deposited alumina for use in micro- and nano-electromechanical systems *Sensors Actuators A* **130–131** 419–29
- [23] Miller D C *et al* 2010 Thermo-mechanical properties of alumina films created using the atomic layer deposition technique *Sensors Actuators A* **164** 58–67
- [24] Prodanovic V *et al* 2015 Science direct optimization of silicon-rich silicon nitride films for electron multiplication in timed photon counters *Proc. Eng.* **120** 1111–4
- [25] Puurunen R L, Saarilahti J and Kattelus H 2007 Implementing ALD layers in MEMS processing *ECS Trans.* **11** 3–14 ecst.ecsdl.org/content/11/7/3.full.pdf
- [26] Aguilar-Gama M T *et al* 2015 Structure and refractive index of thin alumina films grown by atomic layer deposition *J. Mater. Sci. Mater. Electron.* **26** 5546–52
- [27] van Hemmen J L *et al* 2007 Plasma and thermal ALD of Al₂O₃ in a commercial 200 mm ALD reactor *J. Electrochem. Soc.* **154** G165
- [28] Rafi J M, Zabala M, Beldarrain O and Campabadal F 2011 Deposition temperature and thermal annealing effects on the electrical characteristics of atomic layer deposited Al₂O₃ films on silicon *J. Electrochem. Soc.* **158** G108
- [29] Haeberle J *et al* 2013 Ellipsometry and XPS comparative studies of thermal and plasma enhanced atomic layer deposited Al₂O₃ films *Beilstein J. Nanotechnol.* **4** 732–42
- [30] Jakschik S, Schroeder U, Hecht T, Gutsche M, Seidl H and Bartha J W 2003 Crystallization behavior of thin ALD-Al₂O₃ films *Thin Solid Films* **425** 216–20